

Next-to-leading order QCD corrections to $HW^\pm\gamma$ production at the LHC

Song Mao^a, Wan Neng^a, Li Gang^{a,*}, Ma Wen-Gan^b, Zhang Ren-You^b, Guo Lei^b, Zhou Ya-Jin^c, and Guo Jian-You^a

^a *School of Physics and Material Science,*

Anhui University, Hefei, Anhui 230039, P.R.China

^b *Department of Modern Physics, University of Science and Technology of China (USTC), Hefei, Anhui 230026, P.R.China and*

^c *School of Physics, Shandong University, Jinan Shandong 250100, P.R. China*

(Dated: April 4, 2024)

Abstract

The Higgs boson production associated with a W -boson and a photon at the Large Hadron Collider (LHC) can be used to probe the coupling between Higgs boson and vector gauge bosons and discover a signature of new physics. We present the precision predictions up to the QCD next-to-leading-order (NLO) in the standard model for this process involving the subsequential weak decays of the final Higgs and W -boson. The dependence of the leading order (LO) and the QCD NLO corrected integrated cross sections on the factorization/renormalization energy scale is studied. We provide the LO and QCD NLO corrected distributions of the transverse momenta and rapidities of final products. We find that the LO cross section is significantly enhanced by the QCD NLO correction, and the K -factor value is obviously related to the physical observables and the phase space regions.

PACS numbers: 11.15.-q, 12.15.-y, 12.38.Bx

*Electronic address: lig2008@mail.ustc.edu.cn

I. INTRODUCTION

The Higgs mechanism plays a crucial role in the standard model (SM). The existence of the Higgs boson makes the breaking of the electroweak (EW) symmetry and generates the masses for fundamental particles [1, 2]. Therefore, studying the Higgs mechanism is one of the main goals of the Large Hadron Collider (LHC). Recently, both ATLAS and CMS collaborations have announced the discovery of a new boson, whose properties are compatible with that of the SM Higgs particle, with mass of $m_H \approx 125 \text{ GeV}$. Both collaborations excluded additional Higgs-like bosons in a large mass range of m_H about 600 GeV [3, 4]. The interpretation of the excesses observed in various production and decay channels, as originating from a single spin-zero particle, was made possible by detailed theoretical predictions for the Higgs boson production and decay rates, see Ref.[5] for an overview.

After the discovery of the Higgs boson, our main task is to determine its properties, such as spin, CP , and couplings. However, these measurements require accurate theoretical predictions for both signal and background. The process $pp \rightarrow HW^\pm\gamma + X$ is one of the important processes in providing detailed information about the coupling between Higgs boson and vector gauge bosons. This process with subsequent decay of final state to leptons, photons and missing energy, provides a background to new physics searches. It also offers the possibility to study the anomalous couplings in quadrilinear vertices, not present at tree-level in the SM such as $H\gamma WW$, which could be directly investigated in this process as it would cause deviations from the predicted signal.

At the LHC, most of the important processes are multi-body final state production processes. It is known that the theoretical predictions beyond the LO for these processes with more than two final particles are necessary in order to test the SM and search for new physics. But the calculations for these processes involving the NLO corrections are very intricate. In the last few years, the phenomenological results including the NLO QCD corrections for triple gauge boson (TGB) production processes at the LHC, such as $pp \rightarrow WW\gamma$, $ZZ\gamma$, $W\gamma\gamma$, $Z\gamma\gamma$, ZZZ , WWZ have been studied [6–9]. However, Higgs productions associated with di-boson at the NLO were studied less, excepted the process $pp \rightarrow H^0W^+W^-$ [10].

In this paper, we make a precision calculation for the process $pp \rightarrow HW^\pm\gamma + X$ at the LHC, including the contributions of the NLO QCD corrections. In section II we give the

calculation description of the LO cross section for the $pp \rightarrow HW^\pm\gamma + X$ process, and the NLO QCD radiative contribution are presented in section III. In section IV we present some numerical results and discussion. Finally a short summary is given.

II. LO CROSS SECTION FOR $pp \rightarrow HW^+\gamma + X$

In the LO and NLO calculations we employ FeynArts 3.4 package[11] to generate Feynman diagrams and their corresponding amplitudes. The amplitude calculations are implemented by applying FormCalc 5.4 programs [12].

Due to the CP -conservation, the cross section for the $qq' \rightarrow HW^-\gamma$ ($qq' = \bar{u}d, \bar{u}s, \bar{c}d, \bar{c}s$) subprocess in the SM should be the same as that for the corresponding charge conjugate subprocess $qq' \rightarrow HW^+\gamma$ ($qq' = u\bar{d}, u\bar{s}, c\bar{d}, c\bar{s}$) at the parton level. Therefore, we present the parton level calculations for the related subprocess $qq' \rightarrow HW^+\gamma$ in this section. By taking the Cabibbo-Kobayashi-Maskawa matrix elements $V_{td} = V_{ts} = V_{ub} = V_{cb} = 0$, the LO contribution to the cross section for the parent process $pp \rightarrow HW^+\gamma + X$ comes from the subprocesses

$$q(p_1) + q'(p_2) \rightarrow H(p_3) + W^+(p_4) + \gamma(p_5), \quad (qq' = u\bar{d}, u\bar{s}, c\bar{d}, c\bar{s}), \quad (1)$$

where p_1, p_2 and p_3, p_4, p_5 represent the four-momenta of the incoming partons and the outgoing H, W^+ and photon, respectively. We use the 't Hooft-Feynman gauge in our calculations. Since the Yukawa coupling strength is proportional to the fermion mass and the masses of u -, d -, s -, and c -quark are relatively small and can be neglected, we ignore the contribution from the Feynman diagrams with internal Higgs boson line. The Feynman diagrams for the subprocess $qq' \rightarrow HW^+\gamma$ at the LO are depicted in Fig.1.

The expression of the LO cross section for the subprocess $qq' \rightarrow HW^+\gamma$ has the form as

$$\hat{\sigma}_{qq'}^0 = \frac{1}{4} \frac{1}{9} \frac{(2\pi)^4}{2\hat{s}} \int \sum_{spin}^{color} |\mathcal{M}_{qq'}^{LO}|^2 d\Omega_3. \quad (2)$$

where the factors $\frac{1}{4}$ and $\frac{1}{9}$ are due to the averaging over the spins and colors of the initial partons, respectively, \hat{s} is the partonic center-of-mass energy squared, and $\mathcal{M}_{qq'}^{LO}$ is the amplitude of all the tree-level diagrams shown in Fig.1. The summation are taken over the spins and colors of all the relevant particles in the $qq' \rightarrow HW^+\gamma$ subprocess. The

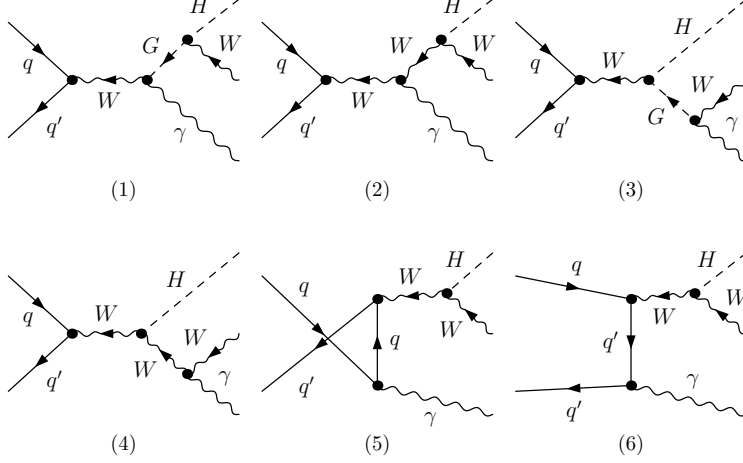


FIG. 1: The LO Feynman diagrams for the partonic process $qq' \rightarrow HW^+\gamma$.

integration is performed over the three-body phase space of the final particles H , W^+ and γ . The phase-space element $d\Omega_3$ in Eq.(2) is expressed as

$$d\Omega_3 = \delta^{(4)} \left(p_1 + p_2 - \sum_{i=3}^5 p_i \right) \prod_{j=3}^5 \frac{d^3 \mathbf{p}_j}{(2\pi)^3 2E_j}. \quad (3)$$

It is obvious that the LO cross section $\hat{\sigma}_{qq'}^0$ is IR divergent when we integrate the Feynman amplitude squared, $|\mathcal{M}_{qq'}^{LO}|^2$, over the full three-body final state phase space. The divergence arises from the integration over the phase space region where the final photon is soft or the photon is radiated from one of the initial massless quarks collinearly. To avoid these IR singularities and obtain an IR-safe result, we should take a transverse momentum cut for final photon (see Sec.4, Eq.(16)). Then the LO total cross section for the parent process $pp \rightarrow HW^+\gamma + X$ at the LHC can be expressed as

$$\sigma_{LO} = \sum_{ij=u\bar{d}, u\bar{s}}^{c\bar{d}, c\bar{s}} \int_0^1 dx_1 \int_0^1 dx_2 [G_{i/P_1}(x_1, \mu_f) G_{j/P_2}(x_2, \mu_f) + (1 \leftrightarrow 2)] \hat{\sigma}_{ij}^0(\hat{s} = x_1 x_2 s), \quad (4)$$

where $G_{i/A}(x, \mu_f)$ is the parton ($i = u, c, \bar{d}, \bar{s}$) distribution function of proton (PDF) $A(= P_1, P_2)$ [13], which describes the probability to find a parton i with momentum $x p_A$ in proton A , s is defined as the total colliding energy squared in proton-proton collision, $\hat{s} = x_1 x_2 s$, and μ_f is the factorization energy scale.

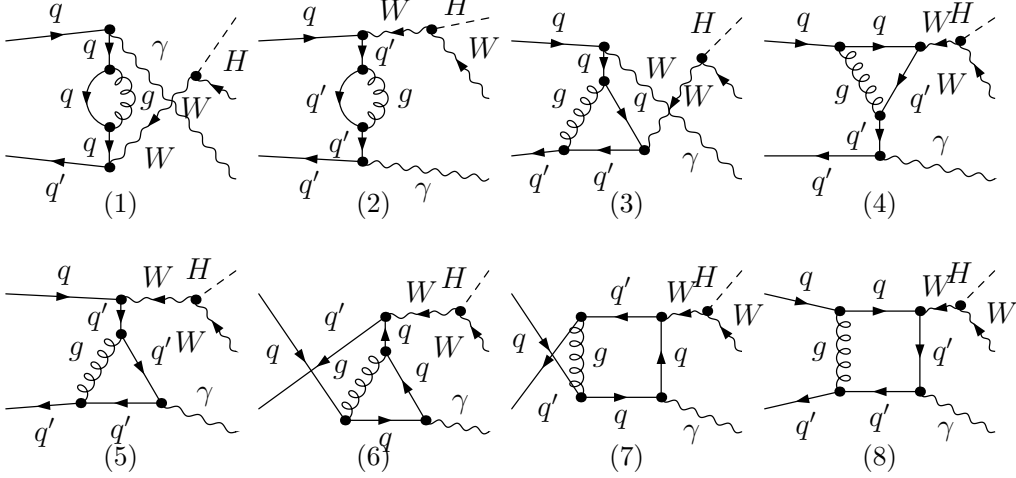


FIG. 2: The representative one-loop Feynman diagrams for the partonic process $qq' \rightarrow HW^+\gamma$.

III. NLO QCD CORRECTIONS TO $pp \rightarrow HW^+\gamma + X$

The $\mathcal{O}(\alpha_s)$ virtual corrections to the partonic $qq' \rightarrow HW^+\gamma$ processes consist of self-energy, vertex, box and pentagon diagrams. Part of these diagrams are presented in Fig.2. We use the definitions of tensor and scalar one-loop integral functions in Ref.[14, 15]. Using the Passarino-Veltman (PV) method [14, 16], the tensor integrals are expressed as a linear combination of tensor structures and coefficients, where the tensor structures depend on the external momenta and the metric tensor, while the coefficients depend on scalar integrals, kinematic invariants and the dimension of the integral.

After the tensor integral reduction is performed, the fundamental building blocks are one-loop scalar integrals. They may be finite or contain both ultraviolet (UV) and infrared (IR) divergences. The UV and IR singular scalar integrals are calculated analytically by using dimensional regularization in $D = 4 - 2\epsilon$ dimensions. We adopt the expressions in Ref.[17] to deal with the IR divergences in Feynman integrals, and apply the expressions in Refs.[18–20] to implement the numerical evaluations for the IR safe parts of N-point integrals. The UV singularities of the virtual corrections are removed by introducing a set of related counterterms. The counterterms are defined as

$$\psi_q^{0,L,R} = \left(1 + \frac{1}{2}\delta Z_q^{L,R}\right) \psi_q^{L,R}, \quad (5)$$

where $\psi_q^{L,R}$ denote the fields of SM quark. The on-mass-shell scheme is adopted to fix the

wave function renormalization constant of the external light quark field, then we obtain

$$\delta Z_q^{L,R} = -\frac{\alpha_s(\mu_R)}{3\pi} [\Delta_{UV} - \Delta_{IR}] , \quad (6)$$

where $\Delta_{UV} = \frac{1}{\epsilon_{UV}} - \gamma_E + \ln(4\pi)$ and $\Delta_{IR} = \frac{1}{\epsilon_{IR}} - \gamma_E + \ln(4\pi)$.

After performing the renormalization procedure, the total NLO QCD amplitude for the subprocess $qq' \rightarrow HW^+\gamma$ is UV finite. Nevertheless, it still contains soft/collinear IR singularities. As we shall see later the soft/collinear IR singularities can be cancelled by adding the contributions of the real gluon/light-(anti)quark emission subprocesses, and redefining the parton distribution functions at the NLO.

According to the Kinoshita-Lee-Nauenberg (KLN) theorem [21] the UV and IR singularities are exactly vanished after combining the renormalized virtual corrections with the contributions of the real gluon emission processes and the PDF counterterms together. These cancelations can be verified numerically in our numerical calculations. The real gluon emission partonic process for the $HW^+\gamma$ can be denoted as

$$q(p_1) + q'(p_2) \rightarrow H(p_3) + W^+(p_4) + \gamma(p_5) + g(p_6), \quad (qq' = u\bar{d}, u\bar{s}, c\bar{d}, c\bar{s}). \quad (7)$$

The real gluon emission subprocess $qq' \rightarrow HW^+\gamma g$ (shown in Fig.3) contains both soft and collinear IR singularities. The IR singularities can be conveniently isolated by adopting the two cutoff phase space slicing (TCPSS) method [22], which is intuitive, simple to implement, and relies on a minimum of process dependent information. The soft IR singularity in the subprocess $qq' \rightarrow HW^+\gamma g$ at the LO cancels the analogous singularity arising from the one-loop level virtual corrections to the $qq' \rightarrow HW^+\gamma$ subprocess.

In performing the calculations with the TCPSS method, we should introduce two arbitrary small cutoffs δ_s and δ_c . The phase space of the $qq' \rightarrow HW^+\gamma g$ subprocess can be split into two regions, $E_6 \leq \delta_s \sqrt{\hat{s}}/2$ (soft gluon region) and $E_6 > \delta_s \sqrt{\hat{s}}/2$ (hard gluon region) by soft cutoff δ_s . The hard gluon region is separated as hard collinear (HC) and hard noncollinear ($\overline{\text{HC}}$) regions by cutoff δ_c . The HC region is the phase space where $-\hat{t}_{16}$ (or $-\hat{t}_{26}$) $< \delta_c \hat{s}$ ($\hat{t}_{16} \equiv (p_1 - p_6)^2$ and $\hat{t}_{26} \equiv (p_2 - p_6)^2$). Then the cross section for the real gluon emission subprocess can be expressed as

$$\hat{\sigma}_g^R(q\bar{q} \rightarrow HW^+\gamma + g) = \hat{\sigma}_g^S + \hat{\sigma}_g^H = \hat{\sigma}_g^S + \hat{\sigma}_g^{\text{HC}} + \hat{\sigma}_g^{\overline{\text{HC}}}. \quad (8)$$

Beside the real gluon emission subprocess discussed above, there is another kind of contribution called the real light-quark emission correction which has the same order contribution

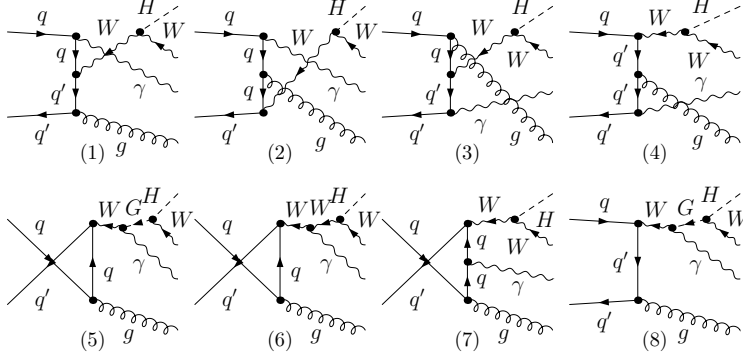


FIG. 3: The representative Feynman diagrams for the real gluon emission subprocess $qq' \rightarrow HW^+\gamma g$.

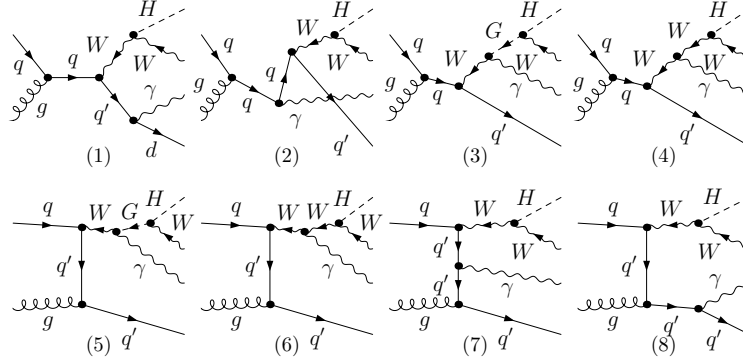


FIG. 4: The representative Feynman diagrams for the real light-quark emission subprocess $qg \rightarrow HW^+\gamma q'$.

with previous real gluon emission subprocess in perturbation theory. The corresponding Feynman diagrams for the subprocess $qg \rightarrow HW^+\gamma q'$ at the tree-level are shown in Fig.4. We denote this subprocess as

$$q(p_1) + g(p_2) \rightarrow H(p_3) + W^+(p_4) + \gamma(p_5) + q'(p_6), \quad (qq' = ud, us, \bar{d}\bar{u}, \bar{s}\bar{c}). \quad (9)$$

It contains only the initial state collinear singularities. Using the TCPSS method described above, we split the phase space into collinear region and noncollinear region by introducing a cutoff δ_c . Then the cross section for the subprocess $qg \rightarrow HW^+\gamma q'$ can be expressed as

$$\hat{\sigma}^R(qg \rightarrow HW^+\gamma q') = \hat{\sigma}_q^R = \hat{\sigma}_q^C + \hat{\sigma}_q^{\bar{C}}. \quad (10)$$

The cross section $\hat{\sigma}_q^{\bar{C}}$ in the noncollinear region is finite and can be evaluated in four

dimensions using Monte Carlo method, while $\hat{\sigma}_q^C$ still contains collinear singularity, which can be absorbed into the redefinition of the PDFs at the NLO.

After adding the renormalized virtual corrections and the real gluon/light-quark emission corrections, the partonic cross sections still contain the collinear divergences, which can be absorbed into the redefinition of the distribution functions at the NLO. We split the PDF counterterm, $\delta G_{i/P}(x, \mu_f)$, into two parts: the collinear gluon emission part $\delta G_{i/P}^{(gluon)}(x, \mu_f)$ and the collinear light-quark emission part $\delta G_{i/P}^{(quark)}(x, \mu_f)$ as

$$\delta G_{q(g)/P}(x, \mu_f) = \delta G_{q(g)/P}^{(gluon)}(x, \mu_f) + \delta G_{q(g)/P}^{(quark)}(x, \mu_f), \quad (q = u, \bar{u}, d, \bar{d}, c, \bar{c}, s, \bar{s}). \quad (11)$$

We get the expressions of the counterterm parts as

$$\begin{aligned} \delta G_{q(g)/P}^{(gluon)}(x, \mu_f) &= \frac{1}{\epsilon} \left[\frac{\alpha_s}{2\pi} \frac{\Gamma(1-\epsilon)}{\Gamma(1-2\epsilon)} \left(\frac{4\pi\mu_r^2}{\mu_f^2} \right)^\epsilon \right] \int_x^1 \frac{dz}{z} P_{qq(gg)}(z) G_{q(g)/P}(x/z, \mu_f), \\ \delta G_{q/P}^{(quark)}(x, \mu_f) &= \frac{1}{\epsilon} \left[\frac{\alpha_s}{2\pi} \frac{\Gamma(1-\epsilon)}{\Gamma(1-2\epsilon)} \left(\frac{4\pi\mu_r^2}{\mu_f^2} \right)^\epsilon \right] \int_x^1 \frac{dz}{z} P_{qg}(z) G_{g/P}(x/z, \mu_f), \\ \delta G_{g/P}^{(quark)}(x, \mu_f) &= \frac{1}{\epsilon} \left[\frac{\alpha_s}{2\pi} \frac{\Gamma(1-\epsilon)}{\Gamma(1-2\epsilon)} \left(\frac{4\pi\mu_r^2}{\mu_f^2} \right)^\epsilon \right] \sum_{q=u, \bar{u}, d, \bar{d}}^{c, \bar{c}, s, \bar{s}} \int_x^1 \frac{dz}{z} P_{gq}(z) G_{q/P}(x/z, \mu_f). \end{aligned} \quad (12)$$

More details about the explicit expressions for the splitting functions $P_{ij}(z)$ ($ij = qq, qg, gq, gg$) are available in Ref.[22].

Finally, we have eliminated all the UV and IR singularities by performing the renormalization procedure and adding all the NLO QCD correction components, and we get the finite NLO QCD corrected integrated cross section for the $pp \rightarrow HW^+\gamma + X$ process as

$$\sigma_{NLO} = \sigma_{LO} + \Delta\sigma_{NLO} = \sigma_{LO} + \Delta\sigma^{(3)} + \Delta\sigma^{(4)}. \quad (13)$$

The three-body term $\Delta\sigma^{(3)}$ includes the one-loop corrections to the process $pp \rightarrow HW^+\gamma + X$ and the tree-level contributions in the soft and hard collinear regions for the real gluon/light-(anti)quark emission processes, while the four-body term $\Delta\sigma^{(4)}$ contains the cross sections for the real gluon/light-(anti)quark emission processes over the hard noncollinear region.

IV. NUMERICAL RESULTS AND DISCUSSION

In this section we present and discuss the numerical results for the $pp \rightarrow HW^\pm\gamma + X$ process at both the LO and the QCD NLO. We adopt the CTEQ6L1 and CTEQ6M parton

densities with five flavors in the LO and NLO calculations, respectively. The strong coupling constant is determined by taking one-loop and two-loop running $\alpha_s(\mu)$ for the LO and the NLO calculations separately, and setting the QCD parameter $\Lambda_5^{LO} = 165 \text{ MeV}$ for the CTEQ6L1 at the LO and $\Lambda_5^{\overline{MS}} = 226 \text{ MeV}$ for the CTEQ6M at the NLO. For simplicity we define the factorization scale and the renormalization scale being equal, and take $\mu \equiv \mu_f = \mu_r = (m_H + m_W)/2$ by default unless stated otherwise. We adopt $m_u = m_d = m_c = m_s = 0$ and employ the following numerical values for the relevant input parameters: [23]

$$\alpha(m_Z)^{-1} = 127.918, \quad m_W = 80.398 \text{ GeV}, \quad m_Z = 91.1876 \text{ GeV}. \quad (14)$$

The CKM matrix elements are fixed as

$$V_{CKM} = \begin{pmatrix} V_{ud} & V_{us} & V_{ub} \\ V_{cd} & V_{cs} & V_{cb} \\ V_{td} & V_{ts} & V_{tb} \end{pmatrix} = \begin{pmatrix} 0.97418 & 0.22577 & 0 \\ -0.22577 & 0.97418 & 0 \\ 0 & 0 & 1 \end{pmatrix}. \quad (15)$$

In order to get rid of the IR singularity from the electroweak sector at the LO, we take the transverse momentum cut on final photon as

$$p_{T_\gamma} > 20 \text{ GeV}. \quad (16)$$

To remove the collinear singularity between the photon and a massless parton i at the NLO calculation, we adopt the selection criterion provided in Ref.[24]. There we accept the $HW^\pm\gamma$ production only if

$$p_{T_i} \leq p_{T_\gamma} \frac{1 - \cos R_{\gamma i}}{1 - \cos \delta_0} \quad \text{or} \quad R_{\gamma i} > \delta_0, \quad (17)$$

where δ_0 is a fixed separation parameter which we set it to be 0.7. The condition of Eq.(17) allows final state partons arbitrarily close to the photon axis as long as they are soft enough. In this way, we can preserve the full QCD singularity, which cancels against the virtual part, but it does not introduce divergences from the interaction between photon and massless quark.

In Figs.5(a,b), the NLO total cross section is plotted against δ_s and δ_c to the $pp \rightarrow HW^\pm\gamma + X$ process at the LHC. The amplified curve for the total correction $\Delta\sigma_{NLO}$ in Fig.5(a) is demonstrated in Fig.5(b) together with calculation errors. Using the TCPSS method, one required $\delta_c \ll \delta_s$. For many calculations it has been found that choosing δ_c to

be 50 - 100 times smaller than δ_s is sufficient for answers accurate to a few percent. Here, we take $\delta_c = \delta_s/50$ and $\mu = \mu_0 = (m_H + m_W)/2$. For the NLO corrections, the virtual and real radiation corrections depend on δ_s and δ_c , separately. However, when all pieces are added together, the dependence on δ_s and δ_c is canceled as long as sufficiently small values of δ_s and δ_c are chosen.

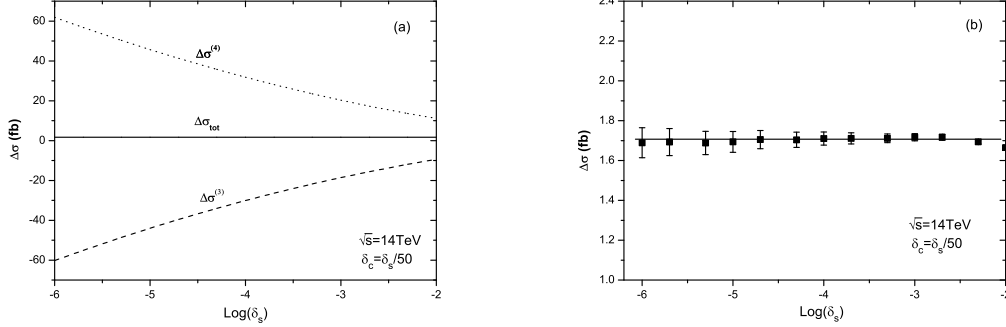


FIG. 5: (a) The dependence of the NLO QCD corrections to the $pp \rightarrow HW^\pm\gamma + X$ process on the cutoffs δ_s and δ_c at the $\sqrt{s} = 14$ TeV LHC, where we take $\delta_c = \delta_s/50$ and $\mu = \mu_0 = (m_H + m_W)/2$. (b) The amplified curve for $\Delta\sigma_{tot}$ in Fig.5(a)

In Fig.6 we illustrate the renormalization and factorization scale dependence of the LO, NLO QCD corrected total cross sections and the corresponding K -factor ($K(\mu) \equiv \sigma_{NLO}(\mu)/\sigma_{LO}(\mu)$) for the process $pp \rightarrow HW^\pm\gamma + X$. We assume $\mu = \mu_r = \mu_f$ and define $\mu_0 = (m_H + m_W)/2$. From this figure, we can see that the LO and NLO QCD corrected total cross section are $4.18fb$ and $5.89fb$ respectively, the corresponding K -factor is 1.41 at $\mu_r = \mu_f = \mu_0$. When the scale μ running from $0.5\mu_0$ to $2\mu_0$, the related theoretical uncertainty amounts to $^{+1.63}_{-2.61}\%$ at the LO and to $^{+3.90}_{-2.88}\%$ at the NLO. It demonstrates that the LO curve underestimates the energy scale dependence. That is because the LO partonic processes for the $pp \rightarrow HW^\pm\gamma + X$ processes are pure electroweak channels where the μ_r dependence is invisible at the LO, the energy scale dependence is the consequence of the parton distribution functions being related to the factorization scale (μ_f).

In Figs.7(a,b,c) we depict the LO and NLO QCD corrected differential cross sections of the transverse momenta for the final produced H -, W^\pm -boson and photon in the process $pp \rightarrow HW^\pm\gamma + X$ at the $14 TeV$ LHC. The differential cross sections of the p_T for H -boson

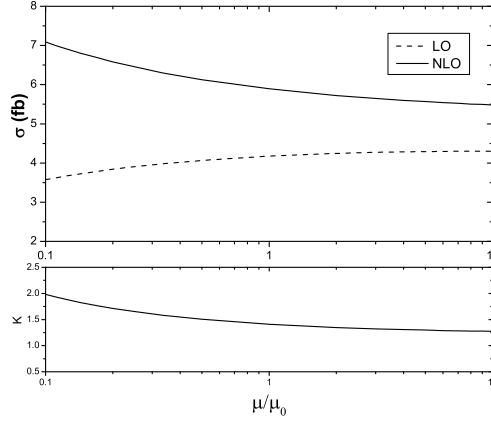


FIG. 6: The dependence of the LO, NLO QCD corrected total cross sections and the corresponding K-factor ($K(\mu) \equiv \sigma_{NLO}(\mu)/\sigma_{LO}(\mu)$) for the process $pp \rightarrow HW^\pm\gamma + X$ on the factorization/renormalization scale (μ/μ_0). Here we assume $\mu = \mu_r = \mu_f$ and define $\mu_0 = (m_H + m_W)/2$.

at the LO and QCD NLO, i.e., $\frac{d\sigma_{LO}}{dp_T^H}$ and $\frac{d\sigma_{NLO}}{dp_T^H}$, are depicted in Fig.7(a), the distributions of $\frac{d\sigma_{LO}}{dp_T^W}$ and $\frac{d\sigma_{NLO}}{dp_T^W}$ for W -boson are plotted in Fig.7(b) and the distributions of $\frac{d\sigma_{LO}}{dp_T^\gamma}$ and $\frac{d\sigma_{NLO}}{dp_T^\gamma}$ for photon are plotted in Fig.7(c) separately. In Figs.7(a) and (b), there exist peaks for the curves of $\frac{d\sigma}{dp_T^H}$ and $\frac{d\sigma}{dp_T^W}$ at the LO and NLO QCD corrections. The peaks are located at the positions around $p_T^H \sim 70 \text{ GeV}$ for Higgs boson and $p_T^W \sim 60 \text{ GeV}$ for W boson. In Fig.7(c), we find that the differential cross section of the photon decreases fast as the increment of the transverse momentum of the photon. We can see from Figs.7(a-c) that all the differential cross sections at the LO for H -, W -boson and photon ($d\sigma_{LO}/dp_T^W$, $d\sigma_{LO}/dp_T^H$, $d\sigma_{LO}/dp_T^\gamma$) are significantly enhanced by the NLO QCD corrections.

As we know, γ can be detected directly in experiment, but H and W^\pm boson are unstable and detected by the signals of their weak decay products. We investigate the kinematic distributions of final products after the subsequent decays of Higgs boson and W gauge boson (i.e., $H \rightarrow \tau^+\tau^-$ and $W^\pm \rightarrow \mu^\pm\nu_\mu$). We employ the SM leptonic decay branch ratios of H and W bosons in further numerical calculations, i.e., $Br(H^0 \rightarrow \tau^+\tau^-) = 6.5\%$ and $Br(W^- \rightarrow \mu^-\bar{\nu}_\mu) = 10.57\%$ [23]. The $HW^+\gamma$ production at the LHC including their subsequent decays can be written as

$$pp \rightarrow HW^\pm\gamma \rightarrow \tau^+\tau^-\mu^\pm \bar{\nu}_\mu^{(-)} \gamma + X. \quad (18)$$

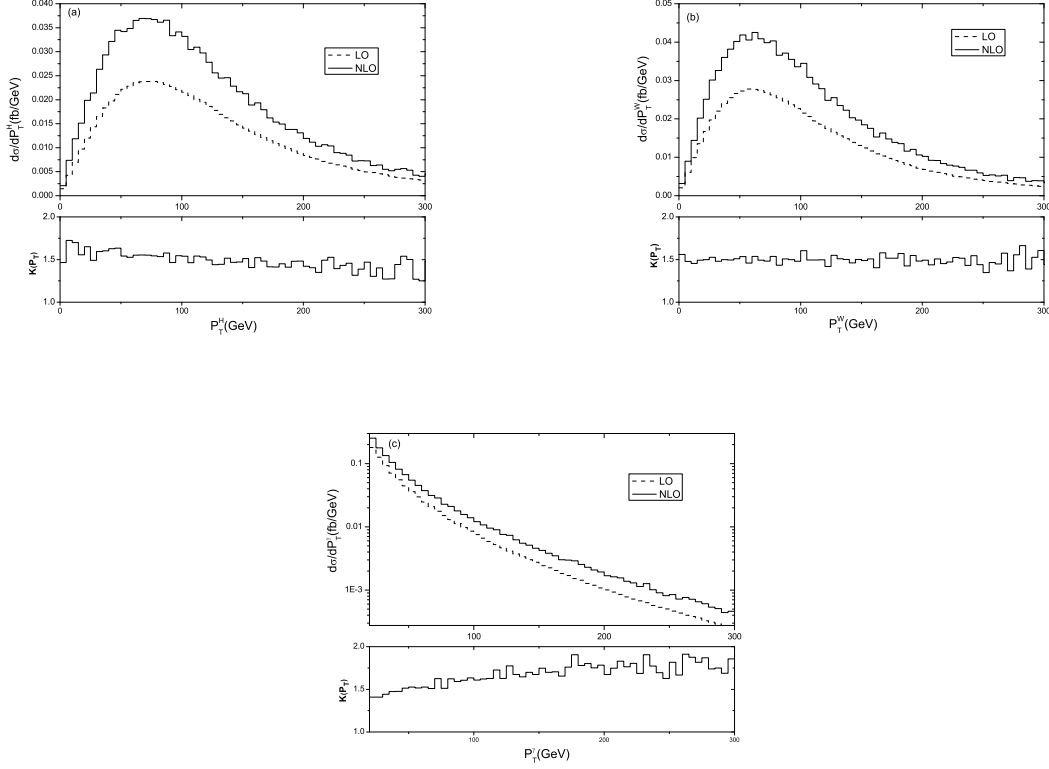


FIG. 7: The LO and QCD NLO distributions of the transverse momenta of final particles and the corresponding K-factors for the $pp \rightarrow HW^\pm\gamma + X$ process at the LHC. (a) for H -boson, (b) for W -boson, (c) for photon.

Then a signal event of $HW^\pm\gamma$ production is detected at the LHC as τ -pair and one charged lepton μ^\pm plus missing energy (ν_μ^-). In Figs.8(a) and (b) we present the LO, NLO QCD corrected distributions of the transverse momentum of τ^+ and μ^\pm , and the corresponding K -factors at the $\sqrt{s} = 14$ TeV LHC, separately. From Figs.8(a,b) we can see that the QCD corrections always enhance the LO differential cross section $d\sigma_{LO}/dp_T^\tau$, and both the LO and QCD NLO corrected distributions of final $\tau(\mu)$ lepton at the future LHC have their peaks at the position of $p_T^{\tau^+} \sim 50$ GeV ($p_T^{\mu^\pm} \sim 25$ GeV), and the $K(p_T)$ -factor value can be beyond 1.50. Figs.8(c) and (d) are for the rapidity distributions of τ^+ - and μ^\pm -leptons, respectively. We can see from all these four figures that the NLO QCD corrections do not make shape change in the transverse momentum and rapidity distributions, while the NLO QCD corrections enhance the LO differential cross sections significantly in all the plotted kinematic regions, and the $K(y_T)$ -factors for lepton τ^+ and μ^\pm can go beyond the values of

1.50 and 1.70, respectively.

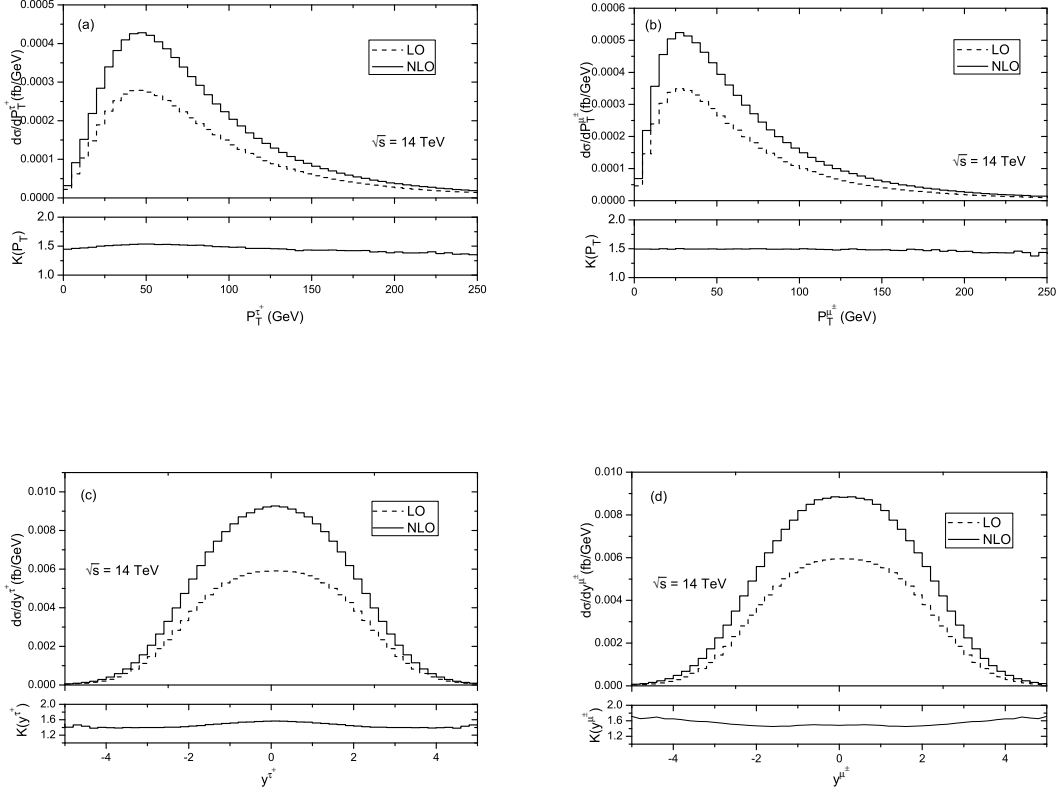


FIG. 8: The LO and NLO QCD corrected distributions of the transverse momenta and rapidity distributions of the final τ^+ - and μ^\pm -leptons and the corresponding K -factors for the $pp \rightarrow HW^\pm\gamma + X \rightarrow \tau^+\tau^-\mu^\pm\nu_\mu\gamma + X$ processes at the $\sqrt{s} = 14$ TeV LHC. (a) $p_T^{\tau^+}$ distributions for final lepton τ^+ , (b) $p_T^{\mu^\pm}$ distributions for final lepton μ^\pm , (c) $y_T^{\tau^+}$ distributions for final lepton τ^+ , (d) $y_T^{\mu^\pm}$ distributions for final lepton μ^\pm .

V. SUMMARY

In this paper we investigate the phenomenological effects induced by the NLO QCD corrections in the Higgs boson production associated with a W -boson and a photon at the LHC.

We present the dependence of the LO and the NLO QCD corrected cross sections on the factorization/renormalization energy scale, and it shows that the scale dependence of the integrated cross section is underestimated by the LO result. We present the LO and the QCD NLO distributions of the transverse momenta and rapidities of final particles. We find that the NLO QCD radiative corrections obviously modify the LO kinematic distributions, and values of K -factor are obviously related to the phase space regions and the kinematic observables. It shows that we should consider the NLO QCD corrections in precision experimental data analyse in studying this process.

VI. ACKNOWLEDGMENTS

This work was supported in part by the National Natural Science Foundation of China (No.11205003, No.11275190, No.11075150, No.11175001, No.11105083), the Key Research Foundation of Education Ministry of Anhui Province of China (No.KJ2012A021), the Youth Foundation of Anhui Province (No.1308085QA07), and financed by the 211 Project of Anhui University (No.02303319).

-
- [1] S. L. Glashow, Nucl. Phys. **22**, (1961) 579; S. Weinberg, Phys. Rev. Lett. **1**, (1967) 1264; A. Salam, Proc. 8th Nobel Symposium Stockholm 1968, ed. N. Svartholm (Almqvist and Wiksells, Stockholm 1968) p.367; H. D. Politzer, Phys. Rep. **14**, (1974) 129.
 - [2] P. W. Higgs, Phys. Lett. **12**, (1964) 132; Phys. Rev. Lett. **13**, (1964) 508; Phys. Rev. **145**, 1156 (1966); F. Englert and R. Brout, Phys. Rev. Lett. **13**, 321 (1964); G. S. Guralnik, C. R. Hagen and T. W. B. Kibble, Phys. Rev. Lett. **13**, (1964) 585; T. W. B. Kibble, Phys. Rev. **155**, (1967) 1554.
 - [3] G. Aad *et al.* [ATLAS Collaboration], Phys. Lett. **B** 716, 1 (2012), arXiv:1207.7214 [hep-ex].
 - [4] S. Chatrchyan *et al.* [CMS Collaboration], Phys. Lett. **B** 716, 30 (2012), arXiv:1207.7235 [hep-ex].
 - [5] LHC Higgs Cross Section Working Group, A. David, A. Denner, M. Duehrssen, M. Grazzini, C. Grojean, G. Passarino and M. Schumacher *et al.*, arXiv:1209.0040[hep-ph].
 - [6] G. Bozzi, F. Campanario, V. Hankele and D. Zeppenfeld, Phys. Rev. **D** **81**, 094030 (2010),

- arXiv:0911.0438.
- [7] G. Bozzi, F. Campanario, M. Rauch and D. Zeppenfeld, Phys. Rev. **D 83**, 114035 (2011), arXiv:1103.4613.
 - [8] A. Lazopoulos, K. Melnikov and F. Petriello, Phys. Rev. **D 76**(2007)014001, arXiv:hep-ph/0703273.
 - [9] V. Hankele and D. Zeppenfeld, Phys. Lett. **B 661** (2008) 103, arXiv:0712.3544 [hep-ph].
 - [10] Song Mao, Ma Wen-Gan, Zhang Ren-You, Guo Lei, Wang Shao-Ming and Han Liang, Phys. Rev. **D 79**, 054016 (2009), arXiv:0903.2885.
 - [11] T. Hahn, Comput. Phys. Commun. **140** (2001)418.
 - [12] T. Hahn, M. Perez-Victoria, Comput. Phys. Commun. **118** (1999)153.
 - [13] J. Pumplin *et al.*, JHEP 0207, 012 (2002); D. Stump *et al.*, JHEP 0310, 046 (2003).
 - [14] G. Passarino and M.J.G. Veltman, Nucl. Phys. **B 160** (1979) 151.
 - [15] A. Denner and S. Dittmaier, Nucl. Phys. **B 734** (2006) 62.
 - [16] A. Denner, Fortsch. Phys. **41**, 307 (1993).
 - [17] R.K. Ellis and G. Zanderighi, JHEP **02**, (2008) 002.
 - [18] G.'t Hooft and M. Veltman, Nucl. Phys. **B 153** (1979) 365.
 - [19] A. Denner, U Nierste and R Scharf, Nucl. Phys. **B 367** (1991) 637.
 - [20] A. Denner and S. Dittmaier, Nucl. Phys. **B 658** (2003) 175.
 - [21] T. Kinoshita, J. Math. Phys. (N.Y.) **3**, 650 (1962); T. D. Lee and M. Nauenberg, Phys. Rev. **133**, B1549 (1964).
 - [22] B. W. Harris and J.F. Owens, Phys. Rev. **D65** (2002) 094032, hep-ph/0102128.
 - [23] C.Amsler, *et al.*, Phys. Lett. **B 667**,1 (2008).
 - [24] S. Frixione, Phys. Lett. **B 429**, 369 (1998) arXiv:hep-ph/9801442.